Pol. J. Environ. Stud. Vol. 34, No. 6 (2025), 8115-8129
DOI: *10.15244/pjoes/194592* ONLINE PUBLICATION DATE: 2024-12-30

Original Research

Multi-Temporal-InSAR Ground Deformation Mapping of Beijing Subway Network Based on ALOS-2 and Sentinel-1 Data

Chengcheng Huang[1, 2], Lei Tan[2, 3]*, Jinxiu Liu[1], Kai Yan[4]

[1]School of Information Engineering, China University of Geosciences, Beijing, 100083, China
[2]Beijing Municipal Engineering Research Institute, Beijing, 100037, China
[3]School of Electronic and Information Engineering, Beijing Jiaotong University, Beijing, 100044, China
[4]Center for GeoData and Analysis, State Key Laboratory of Remote Sensing Science, Faculty of Geographical Science, Beijing Normal University, Beijing, 100875, China

Received: 7 May 2024
Accepted: 13 October 2024

Abstract

Land subsidence is a geological process that occurs at a slow and persistent pace. However, due to the limited archive of high-resolution SAR images, the single-sensor Multi-temporal Interferometric Synthetic Aperture Radar (MTInSAR) technology is unable to satisfy the demands of long-term and high-resolution deformation monitoring. To address this issue, we employed a Small Baseline Subset of InSAR technology, using ALOS-2 and Sentinel-1 data, to detect the deformation characteristics of the Beijing Subway Network (BSN). The two datasets produced consistent results regarding the evolution process and spatial distribution. Subsidence monitoring can be sustained using other datasets when high-resolution images are insufficient. To investigate the differences in deformation characteristics at different stages, we focused on the newly opened section of Beijing Subway Line 17 (L17). Our findings revealed that the southern portion of L17 posed a significant risk of instability with subsidence occurring at Jiahuihu Station, Ciqu Station, and Ciqubei Station. The deformation at these stations was 12.8 mm, 18.7 mm, and 5.6 mm, respectively. Before and after the opening of L17, their deformation rates changed. Specifically, the deformation rate at Jiahuihu Station decreased from -9.4 mm/year to -5.5 mm/year, the deformation rate at Ciqu Station decreased from -14.1 mm/year to -7.5 mm/year, and the deformation rate at Ciqubei Station decreased from -4.9 mm/year to -1.5 mm/year. These results indicate that, after the subway's opening, the deformation rates at these stations are decreasing. The deformation along the subway will intensify during construction and then gradually stabilize once it is operational.

Keywords: SBAS-InSAR, land subsidence, multi-sensor, Beijing subway network, ALOS-2

*e-mail: tanlei_bj@126.com

Introduction

Land subsidence disasters are significant geological hazards that affect numerous countries worldwide [1]. Particularly, cities that have achieved a higher level of internationalization and urbanization are more susceptible to land subsidence. Land subsidence occurs when loose rock layers are compressed and consolidated by natural forces or human activities [2], leading to a reduction in ground elevation in a specific region. It is a slow and persistent geological process [3]. However, when the deformation rate accelerates, it can cause various issues such as house cracking and changes in drainage direction, ultimately resulting in urban waterlogging [4].

Today, more than 200 cities worldwide have built subways, many of which have encountered serious land subsidence [5]. Beijing is one such city that has experienced subsidence induced by excessive groundwater extraction. The first instance of land subsidence in this region was observed in the Xidan-Dongdan area in 1935 and subsequently spread to other areas [6]. By 1999, a total area of 130 km^2 had experienced over 300 mm of accumulated deformation [7]. Due to rapid urbanization and extensive groundwater use over the years, land subsidence has significantly increased in Beijing, with uneven subsidence being more prominent. This poses a serious threat to the safety of linear projects such as subways, making it crucial to analyze the temporal and spatial deformation properties for urban development [8].

Conventional subsidence detection technologies such as level measurement and Global Navigation Satellite System (GNSS) deformation monitoring have been widely utilized to monitor land deformation [9, 10]. However, these methods are limited in their ability to measure real data in planar regions and have low spatial resolution. As a supplement to traditional Interferometric Synthetic Aperture Radar (InSAR) methods, time-series InSAR technology uses radar phase information from multiple SAR images collected at different time periods in the same region, along with radar parameters and satellite position information, to perform interferometric processing and retrieve surface elevation and deformation information [11, 12]. Compared to conventional approaches, time-series InSAR methods are less influenced by low spatiotemporal coherence and atmospheric delay, improving measurement resolution from the centimeter level to the millimeter level and enabling the acquisition of high-precision land deformation and elevation values [13]. There is a good track record demonstrating that these techniques are effective in characterizing large-area surface motions [14, 15].

Permanent Scatterer Interferometry (PSI) and Small Baseline Subset (SBAS) approaches were developed based on traditional Differential Synthetic Aperture Radar Interferometry (DInSAR) [16-19]. SBAS technology is effective for monitoring land subsidence, particularly in urban regions [14]. To achieve high-precision and long-term monitoring using InSAR, high-resolution SAR satellites such as TerraSAR-X (launched by Germany on June 15, 2007) and the ALOS-2 satellite (launched by Japan on May 24, 2014) have been operated [20, 21]. Such satellites have broad potential for monitoring the deformation of large artificial linear objects such as railways and subways [22, 23]. However, two significant challenges remain in achieving high-precision, long-term continuous surface deformation monitoring for linear objects. Firstly, the launch cost of high-resolution SAR satellites is expensive and cannot be ignored. Secondly, the availability of archived high-resolution SAR images is often constrained, and the single-sensor multi-temporal InSAR (MTInSAR) technology may no longer meet the needs of long-term deformation monitoring along subway lines. Multi-sensor, multi-temporal InSAR monitoring technology is expected to effectively meet the requirements for long-term continuous deformation monitoring along subway lines, overcoming the limitation of insufficient archived high-resolution SAR image data.

The paper utilized 12 ALOS-2 SAR images (from March 2021 to June 2022) and 15 Sentinel-1 SAR images (from January 2022 to November 2022) with a time overlap of 6 months, covering the two years before and after the operation of Beijing Subway Line 17 (L17). Using SBAS-InSAR technology, we were able to produce time-series deformation results and average displacement rates for the main urban areas of Beijing. The deformation features along the subway line in Beijing from March 2021 to November 2022 were examined. Then, we mainly analyzed the deformation properties of the L17 during various periods and found that the southern section of the L17 experienced significant uneven subsidence. Finally, we draw conclusions based on the full experimental procedure and study findings.

Study Area and Dataset

Study Area

Beijing, situated in the north of the North China Plain with high topography to the northwest and low terrain to the southeast [24], is one of the most at-risk regions for land subsidence in China. The plain area covers approximately 6300 km^2, with an average elevation of 43.5 m. In the Beijing area, alluvial fans mainly consist of coarse gravel and are the primary locations where subsidence largely occurs [7]. Over the past few decades, the uneven deformation characteristics have become increasingly apparent, and groundwater overexploitation remains the primary cause of land subsidence in this area [25]. The two most significant subsidence centers, Laiguangying (LGY) and Dongbalizhuang-Dajiaoting (DBL) have emerged in the eastern part of the Beijing Plain [26].

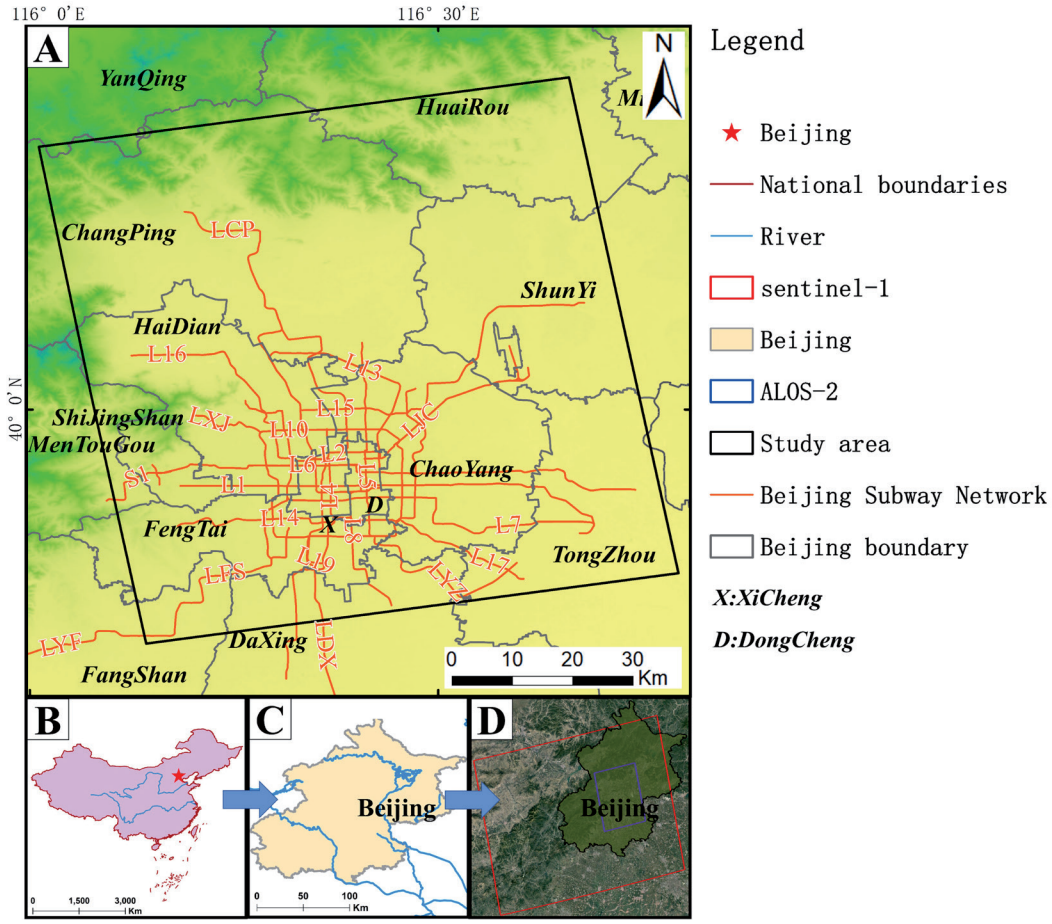

Fig 1. Location of the study area. (a) Distribution of Beijing Subway Network in 2022 is shown by the orange lines; (b) and (c) Location of Beijing Province in China; (d) SAR data range.

Table 1. Acquisition parameters of ALOS-2 and Sentinel-1 datasets.

SAR Sensor	ALOS-2	Sentinel-1
Orbit direction	Ascending	Ascending
Resolution	3 m	15 m
Band (frequency)	L-band (1.2 GHz)	C-band (5.4 GHz)
Revisit cycle	14d	12d
Number of images	12	15
Size of the processed area	55 km*70 km	55 km*70 km
Temporal coverage	March 2021 to June 2022	Jan 2022 to November 2022
Incidence angle	20°~46°	8°~70°
Polarization	HH	VV

On January 15, 1971, the Beijing Subway Network (BSN) inaugurated its first line, making Beijing the first city in China to establish a subway system. As of July 2022, the BSN operated a total of 27 lines with an operating mileage of 783 kilometers. The L17, the 22nd subway line in Beijing, began construction in May 2016 and completed its southern segment (from Jiahuihu Station to Shilihe Station) on December 31, 2021. It spans a length of 15.8 kilometers, encompassing seven stations. Given that almost 2 years have elapsed since the L17 started operating, it is imperative to monitor any ground subsidence along the subway line.

Table 2. Information of ALOS-2 data utilized.

No.	Acquisition data	Orbit	Frame	No.	Acquisition data	Orbit	Frame
1	20210302	36588	0790	9	20211221	40935	0790
2	20210330	37002	0790	10	20220118	41349	0790
3	20210608	38037	0790	11	20220215	41763	0790
4	20210803	38865	0790	12	20220621	43626	0790
5	20210831	39279	0790				
6	20210928	39693	0790				
7	20211026	40107	0790				
8	20211123	40521	0790				

Dataset

In order to monitor deformation along the BSN in 2021–2022, we selected two SAR datasets. The first dataset was the high-resolution ALOS-2 SAR dataset, encompassing the period from March 2021 to June 2022. ALOS-2 was developed as a successor to ALOS-1 by the Japan Aerospace Exploration Agency (JAXA) in response to societal demands [27]. It is currently the only operational L-band SAR satellite, working at a frequency of 1.2 GHz with a wavelength of approximately 23.5 cm [28]. The ALOS-2 satellite, due to its longer wavelength, is better suited for regions with challenging topography and vegetation cover. The Sentinel-1 dataset is another SAR option available for earth observation under the Global Monitoring for Environment and Security (GMES) program [29]. It operates on a C-band SAR with a frequency of 5.4 GHz and a wavelength of around 5.6 cm. Table 1 details the two SAR datasets. Specifically, for this study, the ALOS-2 and Sentinel-1 datasets were captured at incident angles of 39.7° and 42.3°, respectively. The study employed 12 ascending L-band ALOS-2 images in HH polarization, and 15 ascending C-band Sentinel-1 images in VV polarization as depicted in Table 2 and Table 3. Given the limitations in computer resources, processing time, and parallel computing capabilities, we clipped the Sentinel-1 data before conducting InSAR analysis. Fig. 1 illustrates the study area represented by the ALOS-2 black solid data frame, which mainly covered the main urban areas of Beijing. We utilized a digital elevation model (DEM) from the Shuttle Radar Topography Mission (SRTM) at an interval of 1-arc-second for spatial resolution of approximately 30 m × 30 m [30].

Methods

In this study, ALOS-2 and Sentinel-1 SAR images were processed and analyzed using the SBAS-InSAR method. The average deformation rates and time-series deformation results for major urban areas and subway lines in Beijing from 2021 to 2022 were obtained. We further analyzed the variations in deformation characteristics of Beijing Subway Line 17 (L17) across different time periods. Firstly, the slowly-decorrelating filtered phase (SDFP) pixels [31] of the time-series InSAR results obtained from ALOS-2 and Sentinel-1 images were utilized to perform Inverse Distance Weighted (IDW) interpolation. This approach allowed for the acquisition of continuous deformation results in space. Secondly, the deformation features of L17 before and after its opening were investigated using the

Table 3. Information of Sentinel-1 data utilized.

No.	Acquisition data	Orbit	Frame	No.	Acquisition data	Orbit	Frame
1	20220118	41514	126	9	20220717	44139	126
2	20220211	41864	126	10	20220729	44314	126
3	20220223	42039	126	11	20220810	44489	126
4	20220331	42564	126	12	20220927	45189	126
5	20220412	42739	126	13	20221021	45539	126
6	20220506	43089	126	14	20221102	45714	126
7	20220530	43439	126	15	20221114	45889	126
8	20220623	43789	126				

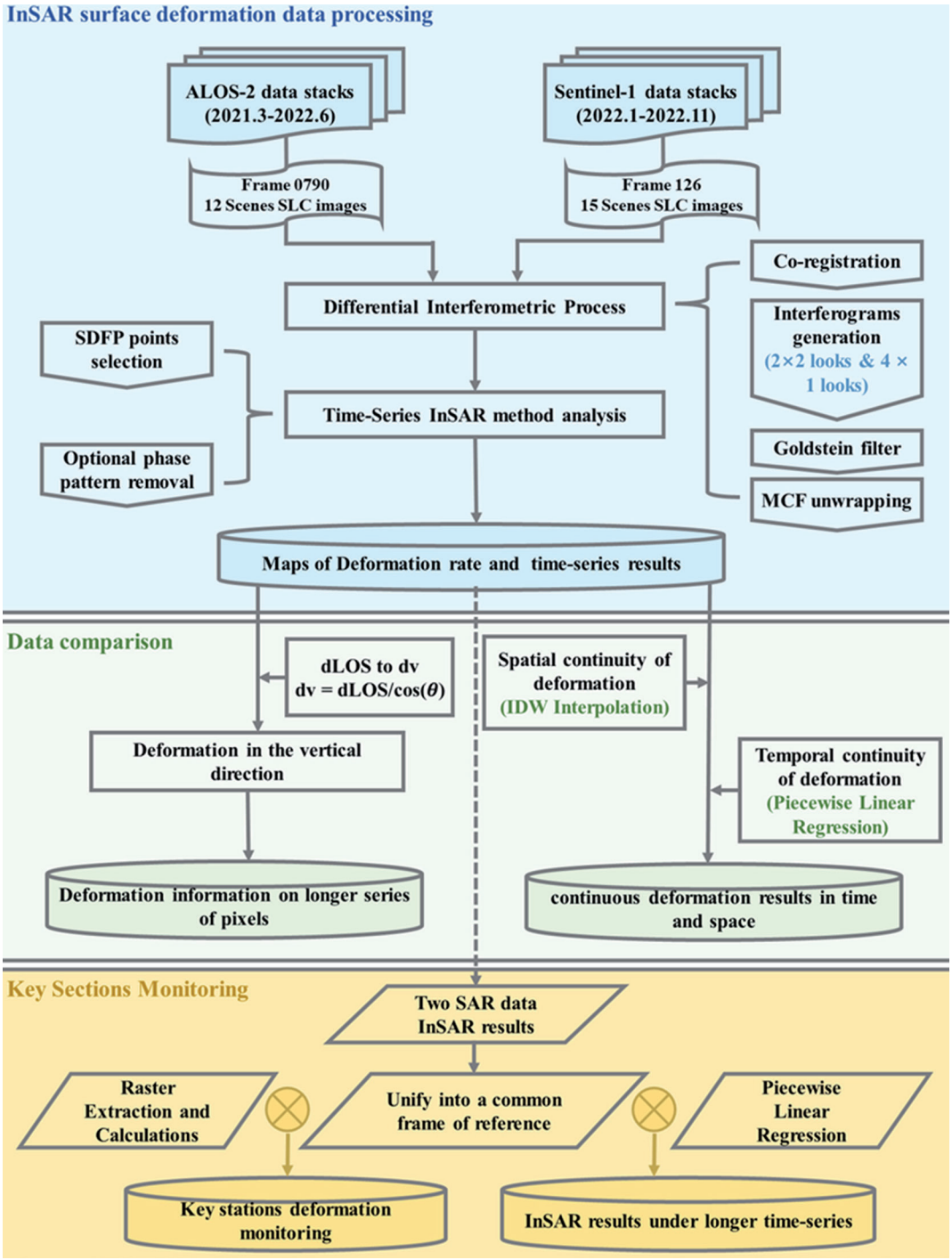

Fig. 2. Workflow of the multi-sensor Multi-temporal InSAR surface deformation data processing and data comparing.

piecewise linear regression technique. We subsequently performed spatiotemporal inversion and mechanism analysis of surface deformation at subway stations, accurately assessing and predicting the stability of L17. Fig. 2 presents an overview of our study. The following sections provide detailed descriptions of the three methods employed.

SBAS-InSAR

The Small Baseline Subset (SBAS) InSAR approach was employed to detect deformation. This technology, suggested by Berardino in 2002 [32], is one of the most commonly used methods. It is a multi-master time-series interferometric stacking technique. To maximize the coherence between interferograms, the SBAS approach reduces the distance of time and Doppler frequencies within images by generating interferograms with multiple small baseline sets [33]. This enhances the

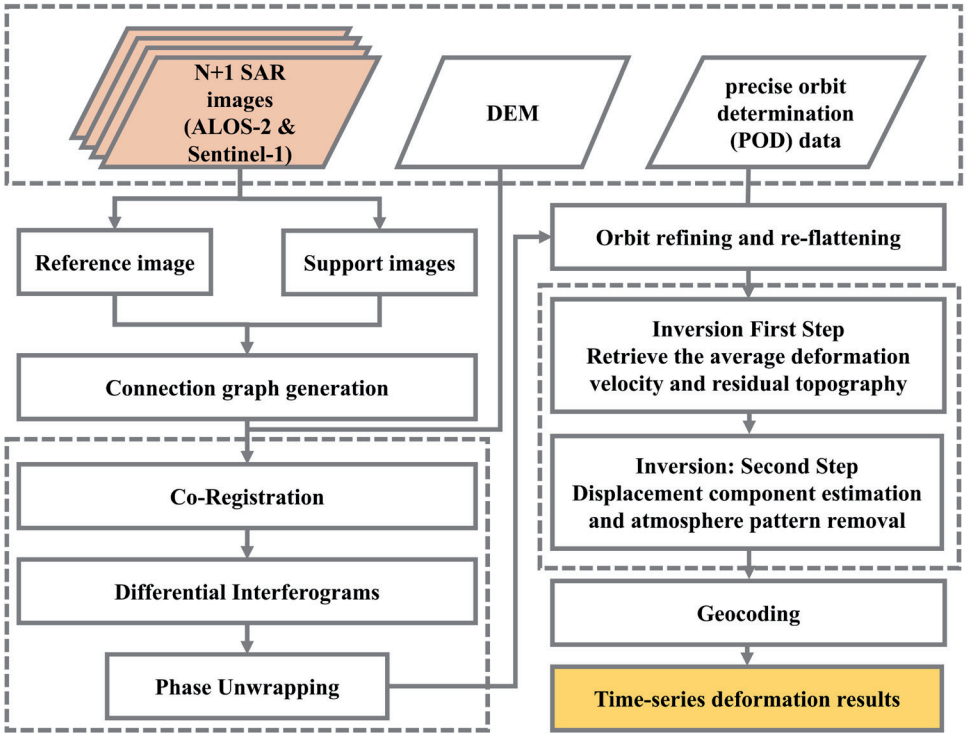

Fig. 3. Logical workflow for the small baseline subset InSAR module.

time sampling rate and adopts an efficient combination of differential interferograms while overcoming spatial decorrelation. The SBAS method achieves an accuracy of 1–2 mm/year in temporal and spatial coherent regions, which is comparable to the measurement accuracy of traditional GPS and PSInSAR [14].

Fig. 3 illustrates the fundamental algorithm flow. The SBAS-InSAR technology consists of four main steps: connection graph generation, interference processing, absolute phase retrieval, and error component removal. Based on the given temporal and spatial baseline thresholds, multiple distinct subsets are generated [34]. Subsequently, the interferometric processing stage produces massive interferograms through a series of steps: master-slave registration of SAR images and generation of differential interferograms. A reference DEM is utilized to eliminate the impact of topography and the flat earth [5]. To remove the noise component in the interferometric phase and achieve a higher ratio of signal-to-noise, the interferograms are filtered. Furthermore, multi-looking processing is conducted on the SAR image stack, which can provide continuous unwrapped phases and more accurate coherence estimations [35]. The spatial correlation between each pair of filtered interferograms is computed to retrieve the unwrapped deformation phase using a phase unwrapping algorithm. To obtain accurate deformed phase measurements, the next step in the SBAS process involves refining and re-flattening the unwrapped phase data stack to remove offsets and trends, as well as separating out other error components [36].

After defining the SAR pair combinations and connecting the network, we generated 37 pairs of differential interferograms using ALOS-2 data and 42 pairs using Sentinel-1 data (as shown in Fig. 4). For the ALOS-2 dataset, we selected the image obtained on August 31, 2021, as the super master image and the other 11 images as slave images. For Sentinel-1, we chose the acquisition on June 23, 2022, as the super master image, with the remaining 14 acquisitions as slave images, all co-registered to this acquisition.

To improve the quality of interferometric phase estimation and reduce radar signal noise, the Goldstein filter method was used to filter the interferograms [37, 38], and multi-looking was taken during interferogram generation. ALOS-2 and Sentinel-1 data were multi-looking processed by 2 × 2 (range × azimuth) and 4 × 1 (range × azimuth), respectively. Precise orbit determination (POD) data from the European Space Agency (ESA) was used for Sentinel-1. The unwrapped phase was processed using the Minimum Cost Flow (MCF) approach and further corrected by selecting and refining steady ground control points [39]. Finally, a specific filter was used to distinguish between atmospheric and deformed phases.

IDW Spatial Interpolation

To address the problem of unwrapped phase discontinuity caused by spatiotemporal decorrelation and random noise, we performed spatial interpolation and raster extraction based on the SDFP points selected from two sets of SAR datasets in the 2 km buffer zone

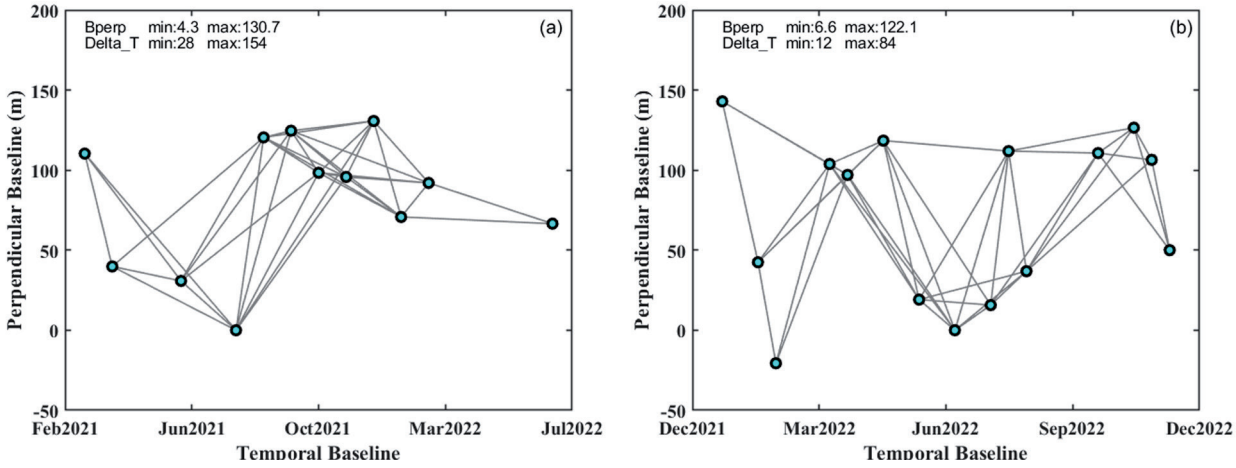

Fig. 4. Baselines of the produced interferograms in terms of space and time: (a) ALOS-2, (b) Sentinel-1.

along L17. In this paper, we adopted the Inverse Distance Weighted Interpolation (IDW) algorithm [40] to obtain spatially continuous InSAR results. This popular and straightforward spatial interpolation technique utilizes the distance between the interpolation points and sample points as the weight, with an inverse relationship between distance and weight value. The formula is as follows:

$$Z_i = \frac{\sum_{i=1}^{n} \frac{1}{d_i^p} Z_j}{\sum_{i=1}^{n} \frac{1}{d_i^p}} \tag{1}$$

In the formula, Z_i represents the value to be interpolated, d_i^p is the distance between the $i-th$ point to be interpolated and the interpolation point, and Z_j denotes the value of the interpolation point itself.

Piecewise Linear Regression

Piecewise linear regression refers to a fitting estimation method applied when the fitting of y to x is in a certain range of x subject to a particular linear relationship, and in other ranges, the linear relationship may have a different slope [41]. To investigate the differences in deformation features of the subway before and after the operation, it is reasonable and effective to perform a piecewise linear regression analysis on InSAR time series results at various stages.

Results and Analysis

We generated time-series InSAR maps of Line of Sight (LOS) deformation from 2021 to 2022 using the SBAS-InSAR method and analyzed the monitoring results. Subsequently, we extracted the deformation data along the BSN. With the aim of understanding the deformation properties before and after the opening of the subway, we converted the deformation result along the LOS direction (dLOS) into the deformation in the vertical direction (dV) based on the incidence angle θ of ALOS-2 and Sentinel-1 images [42, 43]. Our focus was specifically on examining the time-series deformation results at L17 stations, which opened on December 31, 2021.

Mapping and Analysis of InSAR Results

In Fig. 5, we plotted the average deformation rate using ALOS-2 and Sentinel-1 images in the main urban areas of Beijing. The ALOS-2 images were obtained from March 2021 to June 2022, while the Sentinel-1 images covered the period from January 2022 to November 2022. We selected phase-stable pixels as reference points to calculate the deformation rate based on the backscattering signal of the scatterers within the image period. These reference points were marked with a black cross in Fig. 5, and their coordinates were 116.676 E, 39.885 N, and 116.716 E, 40.123 N, respectively. The deformation states of the main urban areas of Beijing can be visually compared across different periods using deformation rates detected by the two SAR datasets. Notably, most of the average deformation rates detected by ALOS-2 images were focused at -30 mm/year ~ 50 mm/year, while those from Sentinel-1 images were mostly at -30 mm/year ~ 15 mm/year. Given that ALOS-2 is an L-band SAR satellite with superior penetration ability and boasts a higher spatial resolution compared to Sentinel-1 data, it is capable of capturing more detailed deformation information pertinent to subsidence. Consistent with prior research, two significant land subsidence areas, S1 and S2, had been monitored [25, 26].

The spatial distribution characteristics of the deformation rate identified by ALOS-2 data and Sentinel-1 data were consistent, showing that most

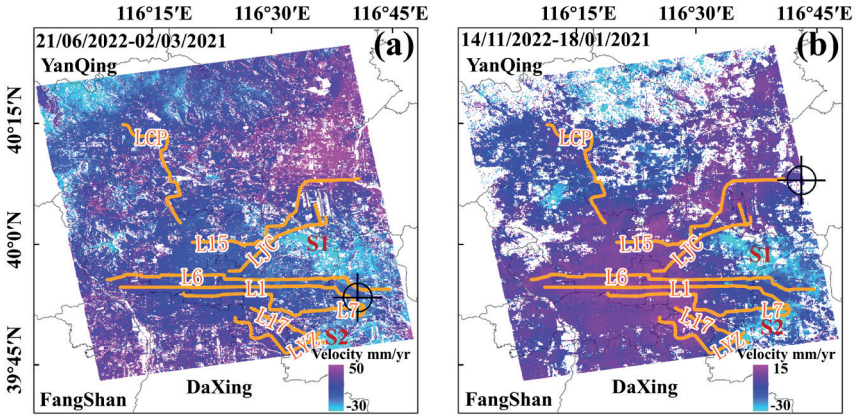

Fig. 5. The Time-series InSAR deformation rates for two types SAR data: (a) ALOS-2, (b) Sentinel-1. The black crosses denote the position of the reference point selected for the deformation monitoring.

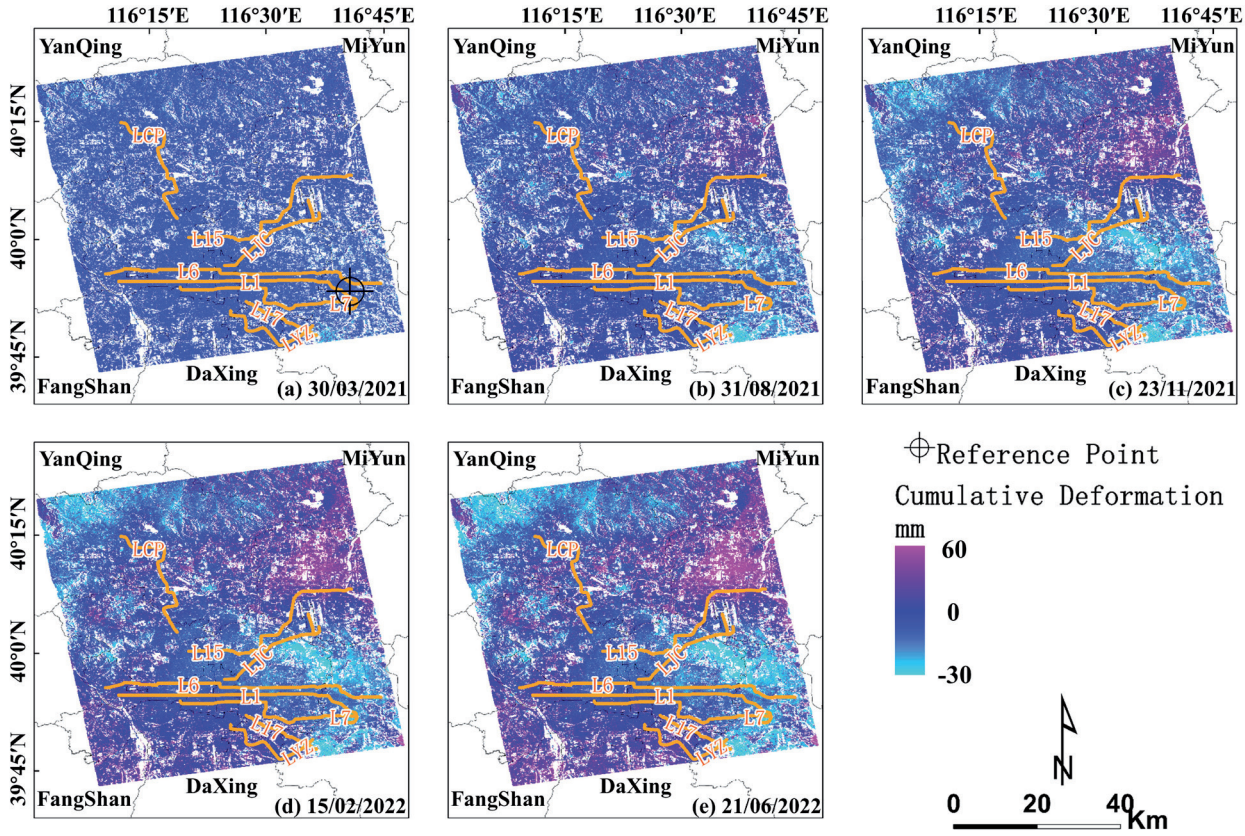

Fig. 6. Mapping of analysis results by ALOS-2 overlaid on time-series evolution of Beijing Subway, from Mar 2021 to Jun 2022.

urban areas were relatively stable but exhibited obvious uneven characteristics in the east-west direction of Beijing. The BSN had seven subway lines (L1, L6, L7, L17, LJC, L15, and LYZ) that traversed two significant subsidence zones. In particular, L17 was newly opened on December 31, 2021. Additionally, two subway lines, namely subway line 1 (L1) and subway line 6 (L6), crossed the eastern and western urban areas, and serious uneven subsidence occurred along these lines. The majority of the eastern sections of L1 and L6 were situated in areas with obvious subsidence, while subsidence throughout the middle and western parts was not apparent. However, based on the deformation rate alone, both lines posed the same safety concerns [24]. For urban linear building facilities, uniform subsidence had minimal impact on safe operation, whereas areas with uneven subsidence or sudden rates of acceleration in deformation are of paramount importance for the future consideration and operation of the subway.

Through the multi-temporal analysis of ALOS-2 and Sentinel-1 SAR data, we plotted the time-series results along the LOS in Fig. 6 and Fig. 7. It can be seen that

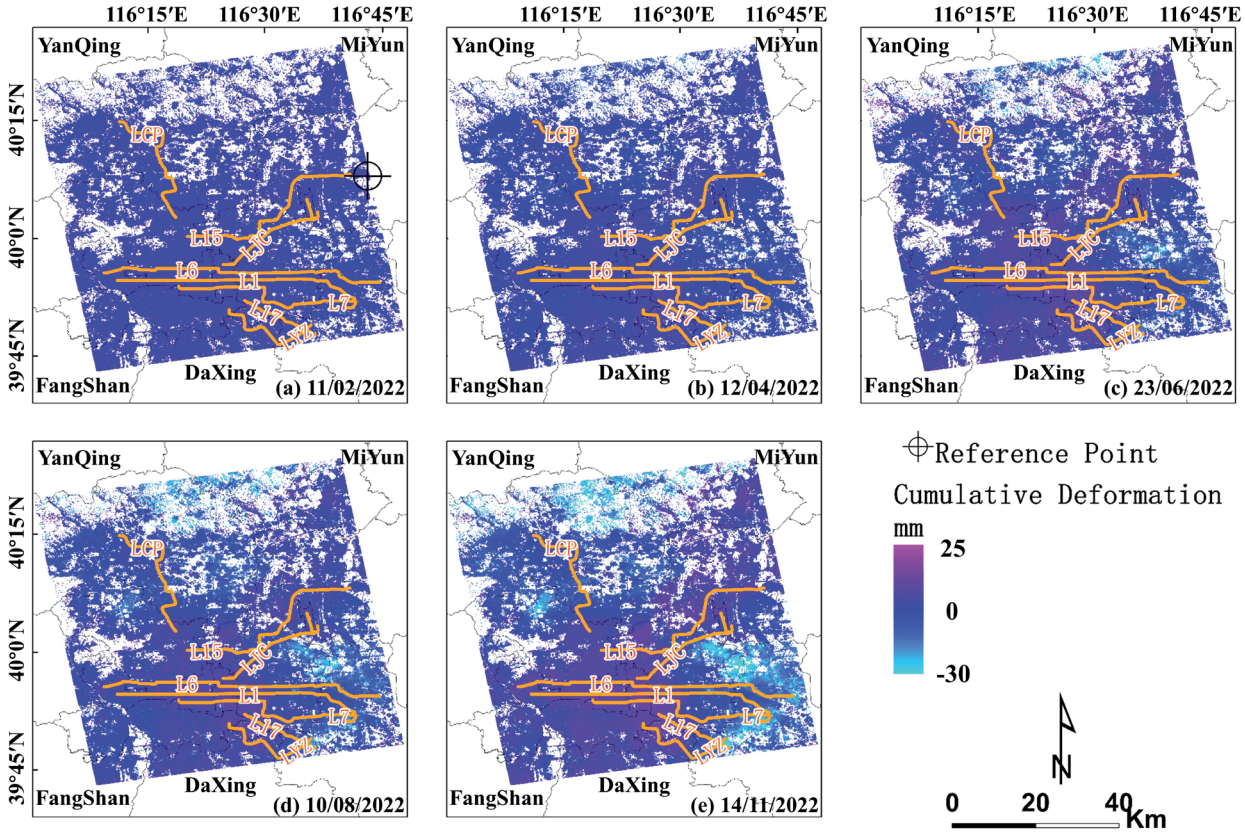

Fig. 7. Mapping of analysis results by Sentinel-1 overlaid on time-series evolution of Beijing Subway, from Jan 2022 to Nov 2022.

from March 2021 to June 2022, the maximum cumulative subsidence rate detected by ALOS-2 data exceeded 30mm, and the most severe areas detected by Sentinel-1 data also experienced a displacement of more than 30 mm between January 2022 and November 2022. The time-series deformation results had intensified, with the displacement values in both S1 and S2 regions gradually increasing. Both the deformation rate and time-series deformation results showed the uneven characteristics of deformation and main deformation areas in the study area. Furthermore, the two deformation measurements at different times demonstrated a comparable geographical pattern and consistent deformation trends across the entirety of Beijing. Thus, when the high-resolution ALOS-2 archived data is insufficient, Sentinel-1 data can be used to continue monitoring the surface subsidence and complete longer-term deformation monitoring along the subway lines.

In addition, based on the rate maps and multi-temporal analysis results obtained from the ALOS-2 and Sentinel-1 datasets, significant ground uplift at a certain scale can be observed in the southern and northeastern regions of the experimental area, with this phenomenon being more pronounced in the rate maps. When using Sentinel-1 data, the ground uplift in the southern region had further expanded into the central part of the study area. This expansion can potentially be attributed to the impact of the Chinese South-to-North Water Diversion (SNWD) Project and various measures implemented to regulate groundwater exploitation in the North China Plain [44, 45]. An increase in groundwater levels in the southern and northeastern sections of the experimental area led to a further reduction of land subsidence.

Beijing Subway Network

To investigate the deformation properties of urban linear infrastructure and understand the impact of ground deformation along the Beijing subway line on subway security and nearby facilities, we extracted time-series InSAR results from within a 600 m buffer zone of the Beijing Subway Network (BSN). The deformation rate results of the BSN detected by ALOS-2 and Sentinel-1 data are presented in Fig. 8. It can be observed that except for a few subway lines passing through subsidence areas, the Beijing Subway Network had no ground subsidence or only a small amount of ground subsidence, and most of the subsidence was uniform. Therefore, the environment along the BSN was stable and did not affect the safe operation of subways.

Most displacement rates along the subway lines detected by ALOS-2 data were concentrated between -30 mm/year and 35 mm/year. Then, most results detected by Sentinel-1 data ranged between -20 mm/year and 15 mm/year. Subway lines experiencing subsidence issues were mainly found in Chaoyang District and Tongzhou District. Affected by the two subsidence centers, there were significant subsidence sections of L1, L6, L7,

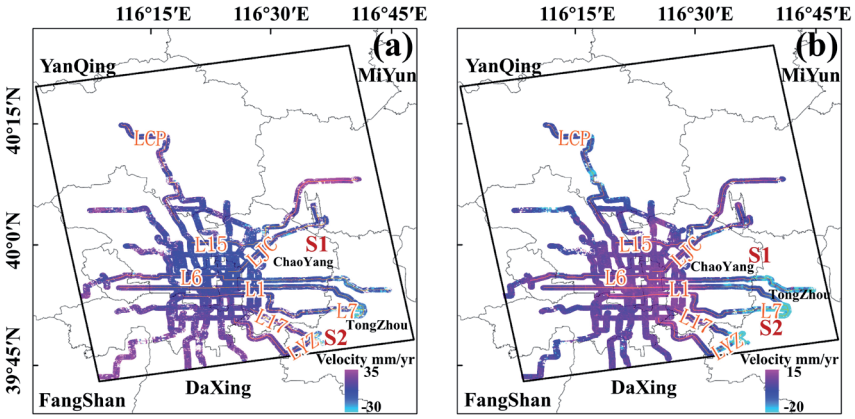

Fig. 8. The average deformation rate of the Beijing Subway Network (within a 600 m buffer zone): (a) ALOS-2, (b) Sentinel-1.

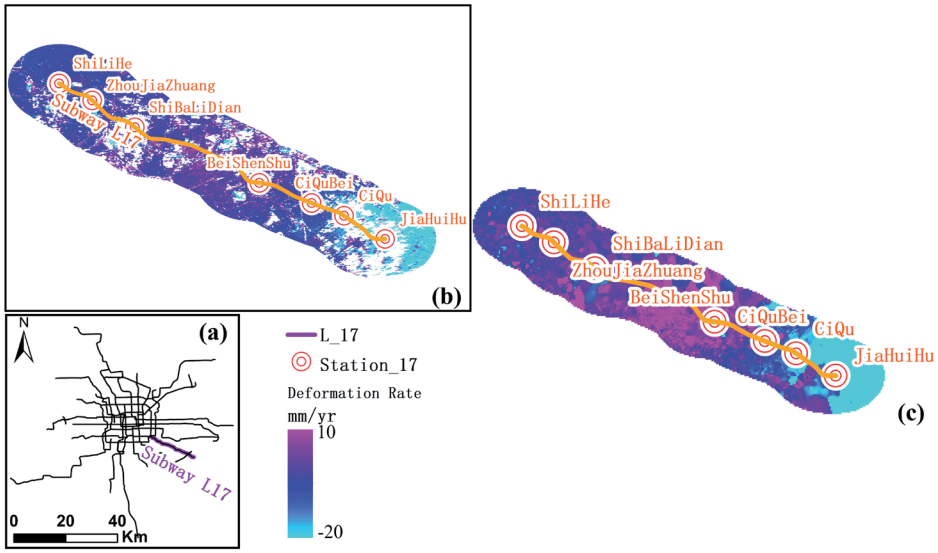

Fig. 9. The left map displays the average vertical deformation rate of the L17 (within a 2 km buffer zone) by ALOS-2, and the right map is the result of the IDW interpolation result.

L17, and Yizhuang Line (LYZ) in the BSN. The most significant uneven subsidence characteristics occurred along L1 and L6. Furthermore, by comparing the SBAS method analysis of two SAR datasets from ALOS-2 and Sentinel-1, it became evident that a new subsidence line had emerged within the midst of the Changping line (LCP) during the monitoring period of Sentinel-1 data.

In general, although the subsidence of the Beijing Subway Network in 2021–2022 was not significant, the continuous occurrence of uneven subsidence remained a threat to the safe operation of BSN. The development of two subsidence centers, S1 and S2, in Chaoyang District and Tongzhou District, respectively, had affected the deformation trend and state along the BSN. It was necessary to stay vigilant about the development of subsidence centers at all times.

Beijing Subway Line 17

As of December 2021, Beijing subway line 17 (L17) had a total length of 15.8 kilometers with 7 stations. It ran through Chaoyang District and Tongzhou District of Beijing in a southeast-northwest direction, from Shilihe Station to Jiahuihu Station. The construction of L17 began in May 2016, and the southern section started operating on December 31, 2021, passing through S2, the largest center of subsidence in Beijing. InSAR is a technology used for side-looking observation, where SAR sensors have varying angles of incidence. To eliminate any discrepancies between ALOS-2 and Sentinel-1 data and analyze the variation in deformation characteristics of each station before and after the running of L17, we converted the Line of Sight (LOS) deformation results into the vertical deformation results.

We compared and analyzed the InSAR results from two datasets by extracting a 2 km buffer around L17 and plotted the deformation rate results of the subway line in

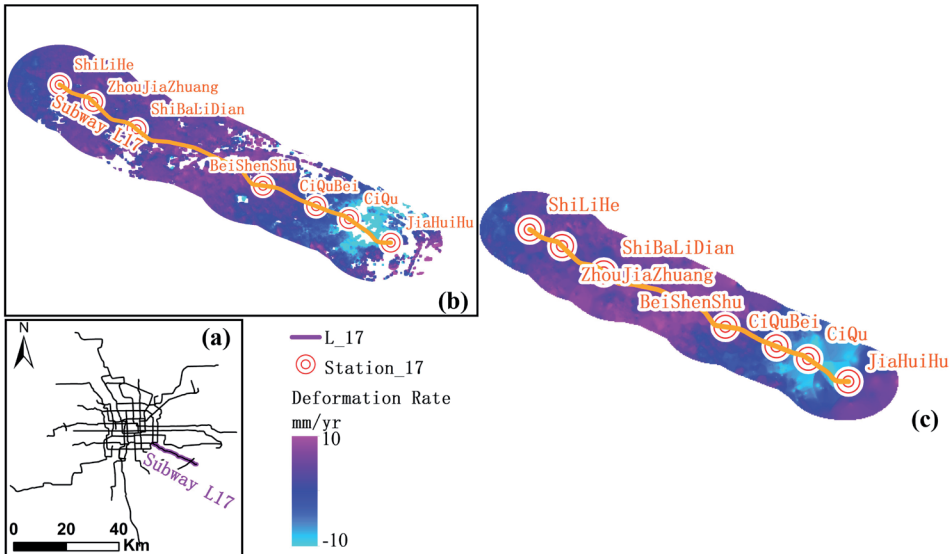

Fig. 10. The left map displays the average vertical deformation rate of the L17 (within a 2 km buffer zone) by Sentinel-1, and the right map is the result of the IDW interpolation result.

Fig. 9b and 10b. However, the time-series InSAR results from the two SAR data could not be obtained in many low-coherence regions within the study area due to unwrapping errors caused by noise and overly extended temporal and spatial baselines. This resulted in a large number of missing data problems, making it challenging to monitor the subsidence characteristics of the subway line.

In order to obtain continuous temporal and spatial time-series InSAR results, we utilized the Inverse Distance Weighted Interpolation (IDW) algorithm for SDFP points located within a 2 km buffer of L17. Our IDW interpolation results were presented in Fig. 9c and Fig. 10c, effectively resolving discontinuities in InSAR results found in low-coherence regions. For ALOS-2 data, the deformation ranged from -20 mm/year to 10 mm/year. Subsidence was primarily concentrated in the southern section of L17. The northern section showed either no substantial subsidence or only a small uniform subsidence. After one year of subway operation, Sentinel-1 data indicated a consistent geographical distribution of deformation features compared to the ALOS-2 data. The subsidence area had remained unchanged, with the majority concentrated in the southern section of the line. The subway stations affected by subsidence were all located in Tongzhou District, and the rate of deformation had decreased, with a deformation rate ranging from -10 mm/year to 10 mm/year. The previously observed uneven subsidence phenomenon had also eased. These findings suggested that urban linear building facilities experienced exacerbated deformation rates and uneven subsidence during the construction period but gradually stabilized during the operation period.

To further verify our conclusion, we calculated time-series results for each subway station using SDFP points within a 100 m buffer around the station. Subsequently, we conducted piecewise linear regression on deformation results before and after subway operation to identify differences in deformation characteristics among stations during various time periods. Since the two SAR data platforms generated short-baseline interference fringes and estimated displacement time-series relative to the first acquisition using SBAS technology, it was necessary to unify the deformation sequences from the two sensors to a common frame of reference. This process enabled us to obtain time-series InSAR deformation information over a longer series of pixels. We adjusted the deformation values for the seven subway stations of L17 by matching the displacement values collected at the corresponding moment in the ALOS-2 data stacks with the point in the first image of Sentinel-1 data stacks acquired on January 18, 2022.

In Fig. 11, we presented the deformation results for seven stations on L17 that had opened: Jiahuihu Station, Ciqu Station, Ciqubei Station, Beishenshu Station, Shibalidian Station, Zhoujiazhuang Station, and Shilihe Station. Additionally, we performed piecewise linear regression on the time-series deformation data of the two SAR data stacks to determine the variations in the deformation rate for each period. The entire time covered by the SAR data stacks, from the opening of L17 on December 31, 2021, was divided into two phases: Phase I, before the opening of the subway, and Phase II, after its opening.

On the whole, the Jiahuihu, Ciqu, and Ciqubei Stations in the southern section of the line experienced subsidence. Among them, the Ciqu Station experienced the most serious land subsidence, followed by Jiahuihu Station and Ciqubei Station, which subsided 18.7 mm, 12.8 mm, and 5.6 mm, respectively. Based on the deformation process observed at Jiahuihu and Ciqu Stations, it was evident that both locations experienced a sustained decline during Phase I and Phase II. However,

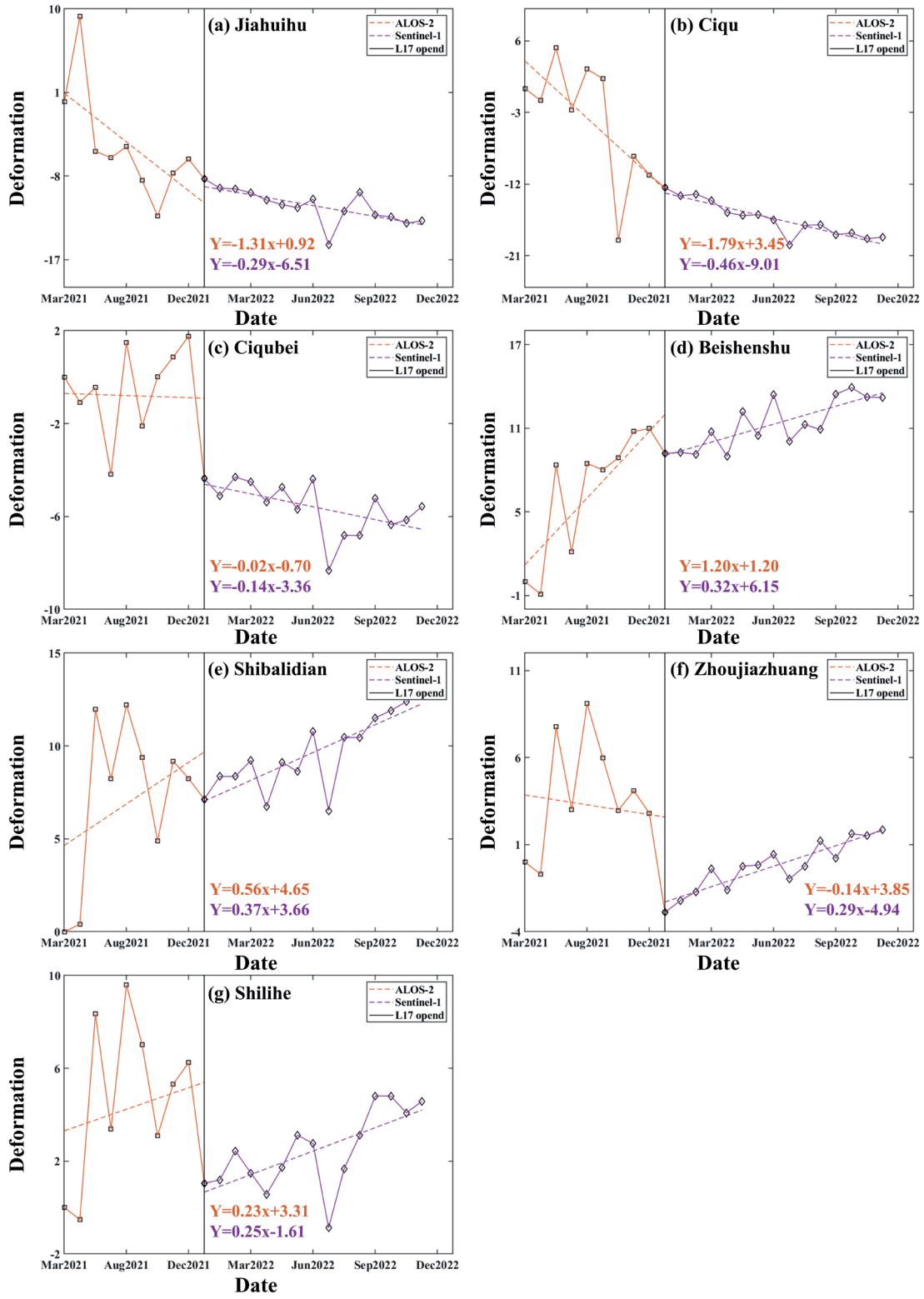

Fig. 11. Linear fitting of subway station subsidence time-series. I: Before operation, II:After operation. (a) Jiahuihu Station, (b) Ciqu station, (c) Ciqubei station, (d) Beishenshu station, (e) Shibalidian station, (f) Zhoujiazhuang station, (g) Shilihe station.

the changing trend in Phase II was weaker than that during Phase I. In contrast, prior to and following the opening of the subway, the subsidence trend at Ciqubei Station remained stable despite an overall decline. The subsidence patterns observed during the data collection periods for ALOS-2 and Sentinel-1 exhibited a similar trend, with the linear fits across various periods being nearly parallel.

Aside from the minor subsidence displacement revealed at Zhoujiazhuang Station in its early days,

no significant ground subsidence phenomena were observed at other stations along L17 prior to its opening. Furthermore, the deformation trend of Beishenshu Station, Shibalidian Station, and Shilihe Station either slowed down or showed only minor changes after the subway line opened. For Beishenshu Station and Shibalidian Station, located in the northern section of L17, the linear trend from January 2022 to November 2022 (Phase II) was lower than that from March 2021 to June 2022 (Phase I). The deformation process exhibited a decreasing trend, with ground deformation tending towards stability. Despite an increase in the deformation rate at Shilihe Station, it remained minimal and posed no threat to the operation of the subway or the safety of surrounding urban municipal facilities.

We utilized the acquisition time of the image on January 18, 2022, as the dividing line to analyze and compare the deformation characteristics of stations that experienced ground subsidence both before and after the subway's opening. The results indicated that, prior to the opening of the subway line, Jiahuihu Station had an average yearly deformation rate of -9.4 mm/year. After its opening, this rate lowered to -5.5 mm/year. Similarly, Ciqu Station had an average yearly deformation rate of -14.1 mm/year before the subway's opening, which decreased to -7.5 mm/year afterward. Ciqu Bei Station's average yearly deformation rate was -4.9 mm/year before the subway opened, lowering to -1.5 mm/year afterward. In terms of the above results, following the construction of L17, the deformation rates at subway stations where subsidence occurred indicated a trend of slowing subsidence and eventual stabilization during operation.

Conclusions

This paper systematically expounded on how to perform InSAR surface deformation data processing and data comparison. Through the incorporation of time-series InSAR technology with multi-sensor and multi-temporal data, we successfully inverted the deformation of the main urban areas within Beijing. We utilized two SAR datasets, ALOS-2 and Sentinel-1, to obtain the time-series InSAR results for the Beijing Subway Network from March 2021 to November 2022 using the SBAS-InSAR method. Additionally, we compared and examined the outcomes from both datasets. The ground deformation measured by SBAS exhibited strong alignment in terms of geographical distribution and development patterns, revealing uneven characteristics of deformation and identifying the primary deformation area within the research field. Hence, these findings affirmed the potential application of multi-source SAR data for continuous monitoring of the same research region. The InSAR results were interpolated using the IDW spatial interpolation algorithm, and piecewise linear fitting was applied to the time-series displacement process of both SAR datasets. Our analysis focused on identifying the differences in subsidence characteristics of the stations before and after the operation of Subway Line 17. We came to the following conclusions:

- The evolution process and spatial distribution of deformation rates for both ALOS-2 and Sentinel-1 were consistent, allowing for realizing long-term InSAR surface deformation monitoring of urban infrastructure, particularly subway lines. The IDW spatial interpolation algorithm was utilized for InSAR results, thus improving the robustness of time-series InSAR technology in regions with low coherence and enabling deformation monitoring results across larger, continuous areas.
- In the main urban areas of Beijing, most areas remained relatively stable, with a yearly average subsidence rate of less than 10 mm/year. The eastern side of Beijing experienced more subsidence than its western side, resulting in noticeable uneven subsidence in the east-west direction. We should give more consideration to the subway lines in east-west distribution and conduct long-term continuous deformation monitoring of these lines, such as L1, L6, and L7. Except for a few subway lines passing through the subsidence centers that experienced obvious subsidence problems, the ground subsidence along the subway lines of the Beijing Subway Network (BSN) was minimal or nonexistent. Furthermore, the monitoring results from the Sentinel-1 SAR dataset indicated an obvious new subsidence section within the midst of the Subway Line Changping.
- During the two years before and after the opening of Beijing Subway Line 17, the three stations situated in the southern section of L17, namely Jiahuihu, Ciqu, and Ciqubei, experienced ground subsidence. All three subway stations were located in Tongzhou District. Following the subway's opening, the rate of deformation at these stations decreased, showing a trend toward slowing subsidence.

Continuous monitoring using multi-source SAR data presented in this paper can be applied to detect deformation features and prevent disasters along urban metro lines, and the results provide reliable scientific evidence for taking proactive measures.

Acknowledgements

The study was made possible by the provision of ALOS-2 and Sentinel-1A data from the Japan Aerospace Exploration Agency (JAXA) (https://www.eorc.jaxa.jp/ALOS/en/alos-2/a2_data_e.htm) and the European Space Agency (ESA) (https://scihub.copernicus.eu), respectively. The precise orbit determination (POD) data used by Sentinel-1 data was downloaded from https://scihub.copernicus.eu/gnss/#/home. We would like to express our gratitude to NASA for providing the SRTM DEM data (https://www.earthdata.nasa.gov/sensors/srtm).

Conflict of Interest

The authors declare no conflict of interest.

Funding

This work was supported by the Technological Innovation Project of Beijing Municipal Engineering Research Institute (KJFZ-KY-W-22064), the National Natural Science Foundation of China Major Program (42192580), and China University of Geosciences (Beijing) 2024 Postgraduate Education and Teaching Reform Project (JG2024012)

Data Availability Statement

The data that support the findings of this study are available from the corresponding author, [Tan lei], upon reasonable request.

References

1. BAGHERI-GAVKOSH M., HOSSEINI S.M., ATAIE-ASHTIANI B., SOHANI Y., EBRAHIMIAN H., MOROVAT F., ASHRAFI S. Land subsidence: A global challenge. Science of The Total Environment, **778,** 146193, **2021**.
2. DINAR A., ESTEBAN E., CALVO E., HERRERA G., TEATINI P., TOMÁS R., LI Y., EZQUERRO P., ALBIAC J. We lose ground: Global assessment of land subsidence impact extent. Science of the Total Environment, **786**, 147415, **2021**.
3. DING Q., SHAO Z., HUANG X., ALTAN O., ZHUANG Q., HU B. Monitoring, analyzing and predicting urban surface subsidence: A case study of Wuhan City, China. International Journal of Applied Earth Observation and Geoinformation, **102**, 102422, **2021**.
4. HU B., LI Z. Time-series InSAR technology for ascending and descending orbital images to monitor surface deformation of the metro network in Chengdu. IEEE Journal of Selected Topics in Applied Earth Observations and Remote Sensing, **14**, 12583, **2021**.
5. LI M.G., CHEN J.J., XU Y.S., TONG D.G., CAO W.W., SHI Y.J. Effects of groundwater exploitation and recharge on land subsidence and infrastructure settlement patterns in Shanghai. Engineering Geology, **282**, 105995, **2021**.
6. GUO L., GONG H., LI J., ZHU L., XUE A., LIAO L., SUN Y., LI Y., ZHAG Z., HU L., GAO M., ZHOU C., CHENG R., ZHOU J. Understanding uneven land subsidence in Beijing, China, using a novel combination of geophysical prospecting and InSAR. Geophysical Research Letters, **47** (16), e2020GL088676, **2020**.
7. LIU L., YU J., CHEN B., WANG Y. Urban subsidence monitoring by SBAS-InSAR technique with multi-platform SAR images: A case study of Beijing Plain, China. European Journal of Remote Sensing, **53** (sup1), 141, **2020**.
8. WANG S., CHEN Z., ZHNG G., XU Z., LIU Y., YUAN Y. Overview and Analysis of Ground Subsidence along China's Urban Subway Network Based on Synthetic Aperture Radar Interferometry. Remote Sensing, **16** (9), 1548, **2020**.
9. AL-KAFF A., MORENO F.M., JOSÉ L.J.S., GARCÍA F., MARTÍN D., DE LA ESCALERA A., NIEVA A., GARCÉA J.L.M. VBII-UAV: Vision-based infrastructure inspection-UAV. Recent Advances in Information Systems and Technologies, **25**, 221, **2017**.
10. LI S., XU W., LI Z. Review of the SBAS InSAR Time-series algorithms, applications, and challenges. Geodesy and Geodynamics, **13** (2), 114, **2022**.
11. WEI D., WANG S. Settlement monitoring and analysis along Xi'an metro line based on time series insar technology. Progress in Geophysics, **39** (2), 498, **2024**.
12. XUE F., LV X., DOU F., YUN Y. A review of time-series interferometric SAR techniques: A tutorial for surface deformation analysis. IEEE Geoscience and Remote Sensing Magazine, **8** (1), 22, **2020**.
13. CHEN B., GONG H., CHEN Y., LEI K., ZHOU C., SI Y., LI X., PAN Y., GAO M. Investigating land subsidence and its causes along Beijing high-speed railway using multi-platform InSAR and a maximum entropy model. International Journal of Applied Earth Observation and Geoinformation, **96**, 102284, **2021**.
14. GUO H., YUAN Y., WANG J., CUI J., ZHANG D., ZHANG R., CAO Q., LI J., DAI W., BAO H., QIAO B., ZHAO S. Large-scale land subsidence monitoring and prediction based on SBAS-InSAR technology with time-series sentinel-1A satellite data. Remote Sensing, **15** (11), 2843, **2023**.
15. SUN H., PENG H., ZENG M., WANG S., PAN Y., PI P., XUE Z., ZHAO X., ZHANG A., LIU F. Land subsidence in a coastal city based on SBAS-InSAR monitoring: a case study of Zhuhai, China. Remote Sensing, **15** (9), 2424, **2023**.
16. ZHAG P., GUO Z., GUO S., XIA J. Land subsidence monitoring method in regions of variable radar reflection characteristics by integrating PS-InSAR and SBAS-InSAR techniques. Remote Sensing, **14** (14), 3265, **2022**.
17. YAO J., YAO X., LIU X. Landslide detection and mapping based on SBAS-InSAR and PS-InSAR: A case study in Gongjue County, Tibet, China. Remote Sensing, **14** (19), 4728, **2022**.
18. HOOPER A., SEGALL P., ZEBKER H. Persistent scatterer interferometric synthetic aperture radar for crustal deformation analysis, with application to Volcán Alcedo, Galápagos. Journal of Geophysical Research: Solid Earth, **112**, 1, **2007**.
19. MAGHSOUDI Y., VAN DER MEER F., HECKER C., PERISSIN D., SAEPULOH A. Using PS-InSAR to detect surface deformation in geothermal areas of West Java in Indonesia. International Journal of Applied Earth Observation and Geoinformation, **64**, 386, **2018**.
20. LIANG J., DONG J., ZHANG S., ZHAO C., LIU B., YANG L., YAN S., MA X. Discussion on InSAR identification effectivity of potential landslides and factors that influence the effectivity. Remote Sensing, **14** (8), 1952, **2022**.
21. ZHU Y., XING X., CHEN L., YUAN Z., TANG P. Ground subsidence investigation in Fuoshan, China, based on SBAS-InSAR technology with TerraSAR-X images. Applied Sciences, **9** (10), 2038, **2019**.
22. BAADE J., SCHMULLIUS C.C. Interferometric microrelief sensing with TerraSAR-X—First results. IEEE Transactions on Geoscience and Remote Sensing, **48** (2), 965, **2009**.
23. LUO Q., ZHOU G., PERISSIN D. Monitoring of

subsidence along Jingjin inter-city railway with high-resolution TerraSAR-X MT-InSAR analysis. Remote Sensing, **9** (7), 717, **2017**.
24. DUAN L., GONG H., CHEN B., ZHOU C., LEI K., GAO M., YU H., CAO Q., CAO J. An improved multi-sensor MTI time-series fusion method to monitor the subsidence of Beijing subway network during the Past 15 Years. Remote Sensing, **12** (13), 2125, **2020**.
25. BAI Z., WANG Y., BALZ T. Beijing land subsidence revealed using PS-InSAR with long time series TerraSAR-X SAR data. Remote Sensing, **14** (11), 2529, **2022**.
26. ZUO J., GONG H., CHEN B., LIU K., ZHOU C., KE Y. Time-series evolution patterns of land subsidence in the eastern Beijing Plain, China. Remote Sensing, **11** (5), 539, **2019**.
27. OHKI M., MOTOOKA T., ABE T., NAGAI H., TADONO T., KANKAKU Y., SHIMADA M. ALOS-2 mission status updates. IGARSS 2018-2018 IEEE International Geoscience and Remote Sensing Symposium, 4166, **2018**.
28. CAO C., ZHU K., SONG T., BAI J., ZHANG W., CHEN J., SONG S. Comparative study on potential landslide identification with ALOS-2 and sentinel-1A data in heavy forest reach, upstream of the Jinsha River. Remote Sensing, **14** (9), 1962, **2022**.
29. ATTEMA E., DAVIDSON M., SNOEIJ P., ROMMEN B., FLOURY N. Sentinel-1 mission overview. 2009 IEEE International Geoscience and Remote Sensing Symposium, **1**, 36, **2009**.
30. FARR T.G., KOBRICK M. Shuttle Radar Topography Mission produces a wealth of data. Eos, Transactions American Geophysical Union, **81** (48), 583, **2000**.
31. ESMAEILI M., MOTAGH M., HOOPER A. Application of dual-polarimetry SAR images in multitemporal InSAR processing. IEEE Geoscience and Remote Sensing Letters, **14** (9), 1489, **2017**.
32. BERARDINO P., FORNARO G., LANARI R., SANSOSTI E. A new algorithm for surface deformation monitoring based on small baseline differential SAR interferograms. IEEE Transactions on Geoscience and Remote Sensing, **40** (11), 2375, **2002**.
33. CIGNA F., TAPETE D. Sentinel-1 big data processing with P-SBAS InSAR in the geohazards exploitation platform: An experiment on coastal land subsidence and landslides in Italy. Remote Sensing, **13** (5), 885, **2021**.
34. WANG S., ZHANG G., CHEN Z., CUI H., ZHENG Y., XU Z., LI Q. Surface deformation extraction from small baseline subset synthetic aperture radar interferometry (SBAS-InSAR) using coherence-optimized baseline combinations. GIScience & Remote Sensing, **59** (1), 295, **2022**.
35. MORISHITA Y. Effective unwrapping of complicated phases by exploiting multiple interferograms: a case study of the 2016 Kumamoto earthquake. Earth, Planets and Space, **74** (1), 33, **2022**.
36. CHAABANI A., DEFFONTAINES B. Application of the SBAS-DInSAR technique for deformation monitoring in Tunis City and Mornag plain. Geomatics, Natural Hazards and Risk, **11** (1), 1346, **2020**.
37. ALSHAMMARI L., LARGE D.J., BOYD D.S., SOWTER A., ANDERSON R., ANDERSEN R., MARSH S. Long-term peatland condition assessment via surface motion monitoring using the ISBAS DInSAR technique over the Flow Country, Scotland. Remote Sensing, **10** (7), 1103, **2018**.
38. GOLDSTEIN R.M., WERNER C.L. Radar interferogram filtering for geophysical applications. Geophysical Research Letters, **25** (21), 4035, **1998**.
39. SHI W., CHEN G., MENG X., JIANG W., CHONG Y., ZHANG Y., DONG Y., ZHANG M. Spatial-temporal evolution of land subsidence and rebound over Xi'an in western China revealed by SBAS-InSAR analysis. Remote Sensing, **12** (22), 3756, **2020**.
40. SHEPARD D. A two-dimensional interpolation function for irregularly-spaced data. Proceedings of the 1968 23rd ACM national conference, 517, **1968**.
41. VAN BOKHOVEN W.M.G. Piecewise-linear modelling and analysis. Eindhoven, Proefschrift, **1981**.
42. CHEN G., ZHANG Y., ZENG R., YANG Z., CHEN X., ZHAO F., MENG X. Detection of Land Subsidence Associated with Land Creation and Rapid Urbanization in the Chinese Loess Plateau Using Time Series InSAR: A Case Study of Lanzhou New District. Remote Sensing, **10** (2), 270, **2018**.
43. ZHANG J., KE C., SHEN X., LIN J., WANG R. Monitoring Land Subsidence along the Subways in Shanghai on the Basis of Time-Series InSAR. Remote Sensing, **15** (4), 908, **2023**.
44. WANG N., DONG J., WANG Z., LEI J., ZHANG L., LIAO M. Monitoring Large-Scale Hydraulic Engineering Using Sentinel-1 InSAR: A Case Study of China's South-to-North Water Diversion Middle Route Project. IEEE Journal of Selected Topics in Applied Earth Observations and Remote Sensing, **15**, 739, **2021**.
45. ZHANG X., CHEN B., GONG H., LEI K., ZHOU C., LU Z., ZHAO D. Inversion of groundwater storage variations considering lag effect in Beijing plain, from Radarsat-2 with SBAS-InSAR Technology. Remote Sensing, **14** (4), 991, **2022**.